drones

MDPI

Article

Droplet Density Optimization of a Drone-Based Air-Assisted Electrostatic Sprayer Using Hybrid Artificial Neural Networks and Ant Colony Optimization Under Laboratory Conditions

Chetan Yumnam †, Satya Prakash Kumar †, Bikram Jyoti *, Ramesh Kumar Sahni *, Manoj Kumar, Karan Singh, Kamal Nayan Agrawal, Shishupal Pal, Avinash Sahu and Manish Kumar

ICAR-Central Institute of Agricultural Engineering, Bhopal 462038, India; yumnamchetan1999@gmail.com (C.Y.); satyaprakash.kr@icar.org.in (S.P.K.)
* Correspondence: bikram.jyoti@icar.org.in (B.J.); ramesh.sahni@wsu.edu (R.K.S.)
† These authors contributed equally to this work.

Highlights

What are the main findings?

- The developed drone-based air-assisted electrostatic spraying system achieved a charge-to-mass ratio of 1.8–2.5 mC/kg and significantly improved droplet density under charged conditions (185.83 ± 4.25 drops/cm^2) compared to uncharged spraying (108.49 ± 2.15 drops/cm^2).
- The ANN–ACO optimization framework successfully identified the optimal operational parameters (FS = 2.58 km/h, PS = 1204 rpm, DR = 558.45 mL/min, AV = 6.18 kV) and demonstrated high prediction accuracy with R^2 values up to 0.9986.

What are the implications of the main findings?

- The drone-based air-assisted electrostatic spraying system produced significantly higher droplet density under charged conditions than uncharged spraying. This suggests the potential for improved spray deposition within the crop canopy. However, canopy penetration, droplet retention, and spray drift were not directly evaluated and require further investigation.
- The integration of ANN with ACO provides a reliable data-driven optimization approach for UAV spraying systems, enabling the development of intelligent, sustainable, and field-efficient drone spraying technologies for modern precision agriculture.

Abstract

Drone-based chemical spraying in agriculture faces challenges related to operator health hazards, spray deposition, application efficiency, and environmental safety. Electrostatic charging system is a novel technology that minimizes off-target spraying losses and increases droplet deposition on the plant canopy. In electrostatic spraying, chemical consumption and application rates are reduced due to the uniform distribution and enhanced deposition of charged droplets on plant surfaces, thereby improving spraying efficacy. In this study, a drone-based air-assisted electrostatic sprayer was developed to investigate the effect of operational parameters that include forward speed, discharge rate, applied voltage (charged condition) and propeller speed on the droplet density (drops/cm^2) in a cotton crop under laboratory conditions. The charge-to-mass ratio (CMR) of the developed air-assisted electrostatic nozzle was found in the range between 1.8–2.5 mC/kg. An Artificial Neural Network–Ant Colony Optimization (ANN–ACO) method was used to optimize the operational parameters for obtaining the highest charged droplet density on the plant

Academic Editors: Jerzy Chojnacki, Simone Pascuzzi and Marcin Siłuch

Received: 18 May 2026
Revised: 21 July 2026
Accepted: 25 July 2026
Published: 27 July 2026

canopy surfaces. Results showed that the charged droplet density was significantly affected by discharge rate (DR) and applied voltage (AV) followed by forward speed (FS) and was slightly influenced by the propeller speed (PS). Optimal performance was achieved at FS = 2.58 km/h, PS = 1204 rpm, DR = 558.45 mL/min and AV = 6.18 kV under the charged conditions. At these optimized parameters, an average charged droplet density of 185.83 ± 4.25 drops/cm^2 (mean ± SE) was achieved. For the uncharged conditions, the optimal performance was achieved at FS = 2.80 km/h, PS = 1065 rpm and DR = 556.75 mL/min, corresponding to an average droplet density of 108.49 ± 2.15 drops/cm^2. The integration of the ANN–ACO optimization algorithm with the drone-based air-assisted electrostatic spraying system can enhance precision chemical application on the cotton, improving efficiency and sustainability.

Keywords: drone; droplet density; electrostatic spraying; cotton; ANN–ACO optimization; precision agriculture

1. Introduction

Conventional pesticide application is resource intensive and poses serious health risks to farmers due to direct exposure through inhalation and skin contact during spray applications. These methods require large volumes of spray liquid, leading to excessive water use, non-uniform chemical deposition, and increased environmental contamination, making them less effective compared to modern spray application techniques [1,2]. In contrast, drone-based spraying offers a precise and efficient alternative, operating with low spray volumes while ensuring uniform and targeted application [3–5]. Drone-based sprayers are particularly suitable for undulated and hilly terrains where interventions are difficult. Precise chemical delivery improves spray efficiency, enhances crop protection, and contributes to increased crop yield and farm income while reducing labor requirements and health risks [6–8].

Conventional drone-based spraying is significantly affected by spray drift caused by environmental factors such as wind, leading to off-target droplet movement and reduced deposition on the crop canopy [9–11]. Drift not only lowers spraying efficiency but also poses serious health risks due to suspended spray droplets in the environment. In addition, non-uniform deposition occurs due to droplet dispersion influenced by spraying height, forward speed, and operational parameters of the drones [12,13]. During spraying, a large proportion of droplets consequently deposit on the soil surface, which is undesirable and may degrade soil quality. Efficient spraying therefore requires improved droplet control and enhanced canopy penetration to maximize on-target deposition on the plant canopy [14–17].

Air-assisted spraying significantly enhances droplet transport and penetration within the plant canopy compared to conventional spraying methods. The introduction of air assistance in combination with an electrostatic charging system further improves droplet penetration and deposition efficiency [17–25]. Electrostatic charging induces an attractive force between the negatively charged spray droplets and the grounded plant surfaces through electromagnetic induction, promoting effective droplet movement toward the canopy [26,27]. As a result, negatively charged droplets adhere to the adaxial and abaxial leaf surface, thereby improving chemical utilization and bio-efficacy [28]. Additionally, the airflow generated in the air-assisted electrostatic system helps to maintain moisture-free charge electrodes preventing back corona droplet impingement on the electrode surface, which is essential for sustaining consistent charging efficiency during spraying operations [22,29,30]. Drone-based air-assisted electrostatic spraying systems enhance the droplet deposition due to the combination effect of airflow and downwash characteristics of the propeller rotational speed, making the charged spray droplets penetrate directly into the plant canopy and covering large areas in short periods of time with minimum chemical input, increasing the efficiency of spraying applications [31].

Recent studies have primarily focused on improving the design and operating characteristics of air-assisted electrostatic spraying systems to enhance droplet charging and deposition performance. Early optimization efforts concentrated on electrostatic nozzle characteristics, where the charge-to-mass ratio (CMR), droplet size, and atomization quality were optimized by adjusting operational parameters such as applied voltage, liquid flow rate, air pressure, spray distance, and electrode configuration. Jyoti et al. (2020) optimized an induction-based electrostatic spray charging system using a Faraday cylinder and obtained a maximum CMR of 1.54 mC/kg at a flow rate of 450 mL/min, an applied voltage of 4.0 kV, and an electrode distance of 40 mm, demonstrating that the optimization of multiple operating parameters is essential for maximizing electrostatic charging performance [3]. Similarly, Dai et al. (2022) reported that increasing air pressure reduced droplet size whereas increasing liquid pressure produced larger droplets, while the CMR increased with applied voltage up to 2.5–3.0 kV before charging efficiency gradually declined [32]. Zhou et al. (2024) improved an air-assisted induction electrostatic nozzle by optimizing air pressure, spray distance, and charging voltage, achieving a maximum CMR of 1.97 mC/kg together with enhanced droplet atomization, canopy penetration, and abaxial leaf deposition [33]. Zhang et al. (2025) developed an air-assisted hollow-cone electrostatic nozzle capable of achieving a CMR of 4.9 mC/kg, improving droplet deposition uniformity, particularly on the abaxial surfaces of soybean leaves [34]. These studies demonstrate the importance of nozzle-level optimization in improving electrostatic spraying performance. Researchers have also evaluated the agronomic performance of air-assisted electrostatic spraying systems. Bueno et al. (2024) reported that combining air assistance with electrostatic charging improved spray deposition, droplet coverage, and soybean yield, with the best performance obtained at an air velocity of 21 m/s and a working speed of 3.3 m/s [20]. Ou et al. (2025) developed a high-clearance air-assisted electrostatic sprayer that increased canopy droplet deposition by 15.72% but penetration into the inner canopy remained limited [23]. Similar improvements in droplet deposition and distribution have also been reported for newly developed UAV electrostatic spraying systems, where electrostatic charging reduced droplet size, increased droplet density, and improved overall deposition compared with conventional spraying. With the increasing adoption of agricultural UAVs, electrostatic spraying technology has been integrated into drone platforms to improve droplet retention and canopy coverage under rotor downwash conditions. Wang et al. (2021) developed a bipolar electrostatic UAV spraying system that increased droplet charge and improved underside leaf deposition through the wrap-around effect without affecting droplet size [35]. Hu et al. (2022) developed an air-assisted electrostatic centrifugal spraying system for UAVs and demonstrated that optimized electrostatic charging increased droplet deposition density and improved distribution uniformity [36]. Zhao et al. (2024) developed a contact-charging electrostatic UAV spraying system that increased droplet density, effective spray width, and overall deposition while enhancing spray coverage through the combined effects of electrostatic forces and propeller-induced airflow [37]. These advance studies have largely focused on optimizing individual nozzle characteristics, charging performance, or deposition behavior using conventional experimental approaches. Limited attention has been devoted to simultaneously optimizing multiple operational parameters of drone-based air-assisted electrostatic spraying systems under rotor downwash conditions. The complex nonlinear interactions among forward speed, propeller speed, discharge rate, applied voltage, and droplet deposition characteristics have rarely been modeled using intelligent optimization techniques.

Proper optimization of operational parameters, including spraying height, forward speed, propeller speed, applied voltage (in charged spraying systems), and liquid discharge rate, is critical for achieving efficient and uniform droplet characteristics [38,39]. Spraying height refers to the vertical distance from the nozzle tip to the top of the crop canopy during the mature growth stage. Forward speed is defined as the horizontal travel velocity of the drone or drone-based simulation platform as it moves linearly above the crop canopy at a specified spraying height during spray application. Propeller speed is defined as the rotational speed of the propeller blades, expressed in revolutions per minute (rpm), which generates the rotor-induced downwash airflow that influences the transport, penetration, and deposition of spray droplets within the crop canopy. Applied voltage is defined as the high-voltage electrical input supplied to the induction electrode of the air-assisted electrostatic nozzle, which induces electrical charge on the spray droplets during atomization. Finally, discharge rate refers to the volumetric flow rate of the spray liquid delivered through the nozzle during operation and is expressed as mL/min. Each parameter directly influences droplet trajectory, droplet distribution, charging efficiency, and canopy penetration, while their combined interactions govern overall spray performance [26]. Sub-optimal parameter selection can result in increased drift, non-uniform deposition, and excessive ground losses [9]. Therefore, innovative optimization approaches coupled with aerodynamic forces, electrostatic interactions, and environmental conditions are essential for better spray droplet characteristics [40].

Conventional optimization approaches such as trial-and-error and single-factor methods are frequently adopted for selecting suitable operational parameters; however, these techniques exhibit several limitations. The trial-and-error approach requires repeated experimental adjustments, making it labor intensive, time consuming, and highly dependent on operator expertise, while offering limited insight into the combined influence of multiple parameters. Similarly, single-factor optimization evaluates individual parameters independently by keeping other variables constant, thereby neglecting the interaction effects among critical factors. In complex spraying systems, where parameters such as spraying height, forward speed, discharge rate, and applied voltage act simultaneously, these methods are inadequate for identifying globally optimal conditions. Consequently, dependence on such optimization techniques often produces sub-optimal performance parameters, increased experimental costs, and reduced reproducibility, underscoring the necessity for multivariate and intelligent optimization strategies [41–43].

A hybrid Artificial Neural Networks–Ant Colony Optimization (ANN–ACO) framework is an intelligent optimization approach to model and optimize complex systems. The ANN acts as a predictive surrogate model, capturing nonlinear relationships between multiple input parameters and system responses [44–46]. The ACO algorithm then uses these predictions to efficiently search for optimal parameter combinations [47–49]. By considering parameter interactions and system nonlinearities, the hybrid ANN–ACO framework overcomes the limitations of conventional optimization methods, reduces experimental effort, and improves optimization accuracy, making it suitable for complex applications such as drone-based and electrostatic spraying systems.

Various nature-inspired optimization techniques have been widely applied independently to optimize system, machine and operational parameters in complex agricultural machine systems. However, the use of these techniques as standalone approaches often results in limited prediction accuracy and typically focuses on the optimization of individual variables, which restricts their ability to capture the complex interactions among multiple operational parameters. Consequently, there remains a need for integrated optimization frameworks capable of simultaneously improving prediction performance and enabling multi-parameter optimization [49,50]. The integration of ANN with ACO provides a promising solution by combining the strong predictive capability of ANN with the global optimization ability of ACO.

Considering the above challenges associated with drone-based spraying, the overall goal of this study was to optimize the operational parameters of a drone-based air-assisted electrostatic spraying system for maximizing droplet density in cotton under laboratory conditions. The specific objectives were to evaluate the effects of forward speed (FS), propeller speed (PS), discharge rate (DR), and applied voltage (AV) on spray deposition characteristics and to determine the optimum operating conditions for enhanced spray performance. The novelty of this study lies in the integration of an air-assisted electrostatic spraying system with a data-driven ANN–ACO framework to simultaneously model and optimize drone-based spraying parameters. Furthermore, the study provides quantitative insights into the chargeability and deposition behaviour of electrostatically charged droplets under different operating conditions. The practical significance of this research is to demonstrate the potential of electrostatic charging combined with air assistance to enhance droplet density, canopy penetration, and spray retention while reducing spray losses, thereby improving the efficiency and sustainability of precision pesticide application. In addition, the proposed ANN–ACO optimization approach offers a reliable decision–support tool for the development of intelligent and field-efficient drone-based spraying technologies for modern precision agriculture.

2. Materials and Methods

2.1. Experimental Site

The experiment was carried out at the Drone System Laboratory, ICAR—Central Institute of Agricultural Engineering, Bhopal (23°18′40.2″ N, 77°24′11.8″ E), in the cotton crop (*Gossypium* spp.) during November 2025. The cotton crop was planted in a vase to conduct the experiment. At the time of experimentation, the crop was at the mature stage, with an average plant height of 1.0 ± 0.10 m (mean ± SD) and a plant-to-plant spacing of 0.75 m. The mean ambient temperature and relative humidity recorded during the experiment were 28.5 ± 2 °C and 48 ± 5%, respectively, which were within the recommended range for spraying operations.

2.2. Drone-Based Simulation Platform

A drone-simulation platform was developed to simulate the spraying operation in controlled conditions for determining the spray droplet characteristics affected by various operational parameters such as forward speed, flight height, propeller speed and discharge rate (Figure 1a). Major components of the platform are a direct current (DC) motor, switch mode power supply (SMPS), brushless direct current (BLDC) motor and spray tank. The simulating platform works such that the trolley is driven by a DC motor coupled with a motor driver and powered through SMPS, allowing precise control over forward speed of the drone platform. The developed drone-based simulation platform was integrated with proximity sensors, magnetic and optical encoders, and flow controllers for real-time monitoring and control of key operational parameters. Furthermore, a safety switch was installed to provide electrical protection and ensure safe operation of the system. Mounted on a trolley, a BLDC motor–propeller assembly generates downward airflow, mimicking the rotor-induced downwash of a drone in field conditions. The spraying system consists of a 10 L spray tank connected to a diaphragm pump that delivers the spray solutions to the nozzle. The discharge rate is regulated using a control knob, enabling variation in the flow rate as per the experimental requirements. The entire system is operated through a Radio Frequency (RF) receiver connected to a Remote Control (RC) controller, allowing real-time adjustment of parameters such as forward speed and propeller speed. The platform dimensions (15 m length, 2 m width and 5 m height) provide sufficient space to simulate field conditions (Figure 1b). Limit switches are installed at both ends of the track to automatically stop the simulation platform and prevent collisions during forward and reverse movement. In addition, springs are provided at both ends as a safety measure to absorb impact and protect the system in cases when the unmanned vehicle trolley overshoots the track limits.

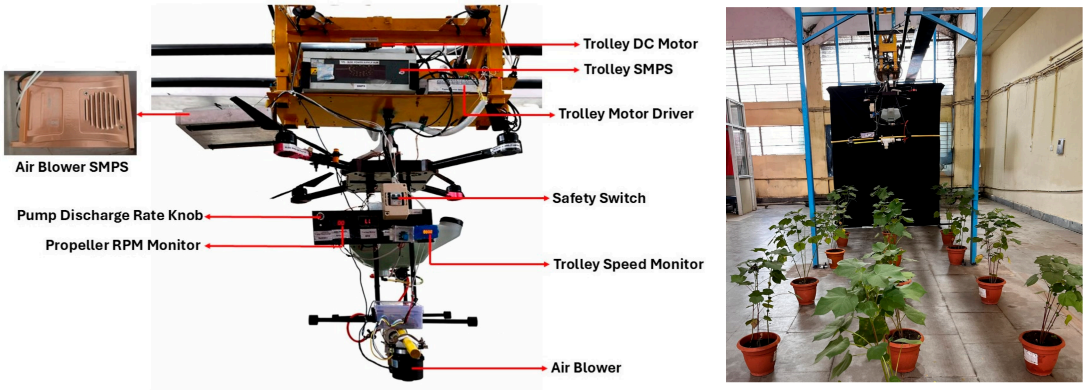

(**a**) (**b**)

Figure 1. Drone simulation platform with various (**a**) components used for (**b**) simulating field conditions in cotton plants.

2.3. Drone-Based Air-Assisted Electrostatic Spraying System

The drone-based air-assisted electrostatic sprayer system was developed to charge the sprayed droplets oozing out from the spraying nozzle (Figure 2). The induction-charging nozzle consisted of a cylindrical aluminum electrode axially mounted around a high-pressure hollow cone nozzle (model: HCN/PB, pressure: 274.58 kPa, discharge rate: 450 mL/min, ASPEE Agro Equipment Pvt. Ltd., Mumbai, MH, India). Aluminum was selected as the electrode material, considering its cost-effectiveness, lightweight nature, and adequate electrical conductivity. Although copper exhibits lower resistivity than aluminum, the difference in electrode resistance has a negligible effect under the low-current operating conditions of this system. Therefore, aluminum provides a practical and economical alternative while maintaining the required electrical performance. When the liquid emerges from the nozzle, it passes through the strong electric field and accumulates charge on the emerging droplets that become attracted to the grounded plant canopy. A high-voltage generator (model: F121, input voltage: 0–15 VDC, output voltage: 0–12,000 VDC, EMCO High Voltage Corporation, Sutter Creek, CA, USA) was connected to the cylindrical electrode to impart the required electric field around the spray droplets. A high-speed air blower (model: WS9290, input voltage: 12 VDC, speed: 22,000 rpm, Wonsmart Motor Fan Co., Ltd., Ningbo, China) powered by SMPS (model: DX-400W, input voltage: 12 V, power: 400 W, current output: 33.3 A, HiLight, Jaipur, India) was used to create a high air density between the electrode and nozzle. The spray liquid was atomized into spray droplets near the nozzle orifice into droplets of size 52.82 to 400.18 µm at a nozzle discharge rate of 488 to 563 mL/min.

https://doi.org/10.3390/drones10080573

Figure 2. Components of a drone-based air-assisted electrostatic spraying system.

2.4. Working Mechanism of a Drone-Based Air-Assisted Electrostatic Spraying System

When the electrode of the nozzle was supplied with the high electrical input using a 12 kV high-voltage generator (model: F121, input voltage: 0–15 VDC, output voltage: 0–12,000 VDC, EMCO High Voltage Corporation, CA, USA), the exposed electrode generates a strong electric field. As atomized droplets pass through the electric field generated between the induction electrode and the grounded target, charge separation occurs within the droplets, resulting in electrostatically charged droplets through an induction charging process. The induction-charging nozzle was operated by applying a positive high voltage to the induction electrode while maintaining electrical insulation between the liquid flow and the charging electrode. Under this configuration, electrons are attracted toward the positively charged induction electrode, resulting in the spray droplets acquiring a net negative charge (Figure 3).

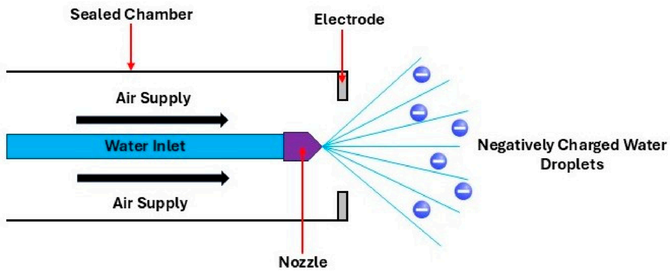

Figure 3. Charging mechanism of electrostatic spraying.

Charged droplets exhibit mutual repulsion, resulting in finer dispersion and improved spray uniformity. As droplets approach grounded crop surfaces, electrostatic attraction governed by Coulombic forces enhances directional movement and deposition efficiency. This interaction promotes the wrap-around effect, enabling deposition on adaxial and abaxial leaf surfaces. The electrical circuit and configuration of the drone-based air-assisted electrostatic spraying system is given below in Figure 4.

2.5. Experimental Design

2.5.1. Description of Faraday Cage Cylinder

To quantify the electrostatic charge accumulated on spray droplets, the Faraday cylinder method was employed following standard procedures. The Faraday cylinder was designed to capture the entire charged spray released at a specific instant, thereby ensuring complete collection of the charge associated with the droplets. The setup comprised a hollow cylindrical chamber fabricated from aluminum sheet material, with dimensions of 900 mm in length and 550 mm in diameter. Three circular stainless-steel sieves (1 mm mesh size) were positioned at equal intervals from the base up to half the cylinder height. These sieves facilitated interception of the charged droplets and enabled transfer of the electrical charge to the conductive body of the cylinder. Charge transfer efficiency was enhanced by increasing the contact area between the spray liquid and the conductive mesh surfaces. An outlet was provided at the bottom of the cylinder for removal of the collected spray liquid when necessary. The entire assembly was mounted on a stand fitted with a rubber insulator to avoid electrical grounding.

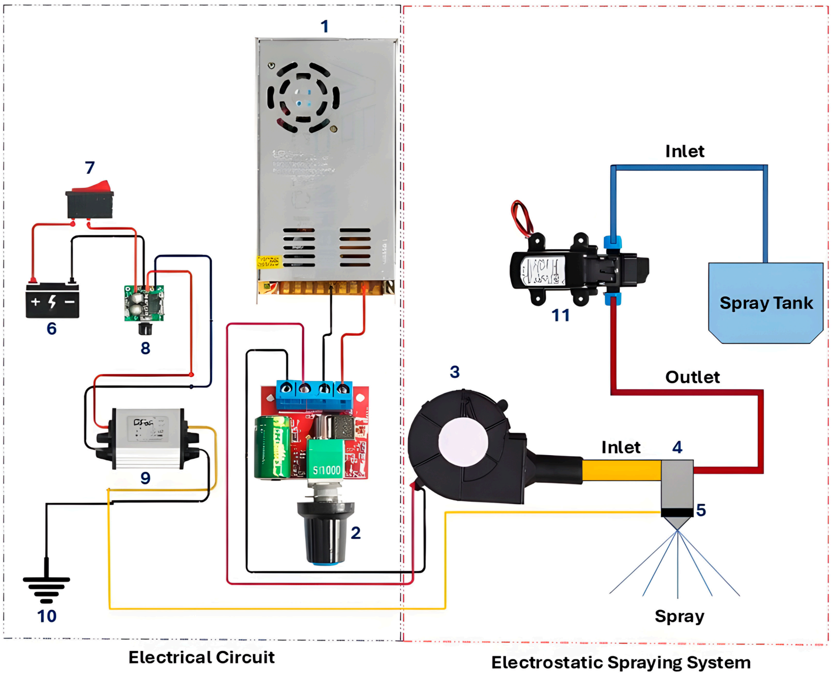

Figure 4. Electrical circuit and configuration of the air-assisted electrostatic spraying system. 1. SMPS; 2. voltage regulator; 3. air blower; 4. nozzle; 5. electrode; 6. battery; 7. switch; 8. voltage regulator module; 9. voltage converter; 10. grounding unit; 11. pump.

2.5.2. Measurement of Charge-to-Mass Ratio (CMR)

The CMR is an important parameter used to evaluate the electrostatic charging performance of a spray nozzle. It is defined as the ratio of charge quantity to mass of droplet deposited [3], as mentioned in Equation (1). A higher CMR generally indicates improved electrostatic deposition efficiency. During the experiment, the CMR of the electrostatic spray nozzle was measured using a cylindrical Faraday cage system (Figure 5a). When charged droplets entered the Faraday cage cylinder, the electrical charge carried by the droplets was transferred to the cylinder surface, producing an electrical current proportional to the droplet charge. The induced spray current was measured using a digital multi-meter (model: 81-USB, Meco Instruments Pvt Ltd., Mumbai, MH, India) (Figure 5a). The positive terminal of the multi-meter was connected to the Faraday cage cylinder, while the negative terminal was grounded to complete the electrical circuit and ensure accurate current measurement. To improve the collection efficiency of charged droplets, the air-assisted electrostatic nozzle was positioned close to the open end of the Faraday cage cylinder (Figure 5b). As the spray droplets accumulated inside the cylinder, the resulting electrical current generated by charge transfer was recorded. Simultaneously, the mass of the collected spray liquid was measured gravimetrically.

The CMR of the electrostatic spray was calculated using the following relationship:

$$\mathrm{CMR} = \frac{I_s}{Q_m} \tag{1}$$

where I_s is the spray charge current (mA) measured from the Faraday cage cylinder and Q_m is the mass flow rate of the sprayed liquid (kg/min). In the Faraday cage cylinder experiment, the CMR for the developed induction-based air-assisted electrostatic nozzle was found to be 1.8–2.5 mC/kg.

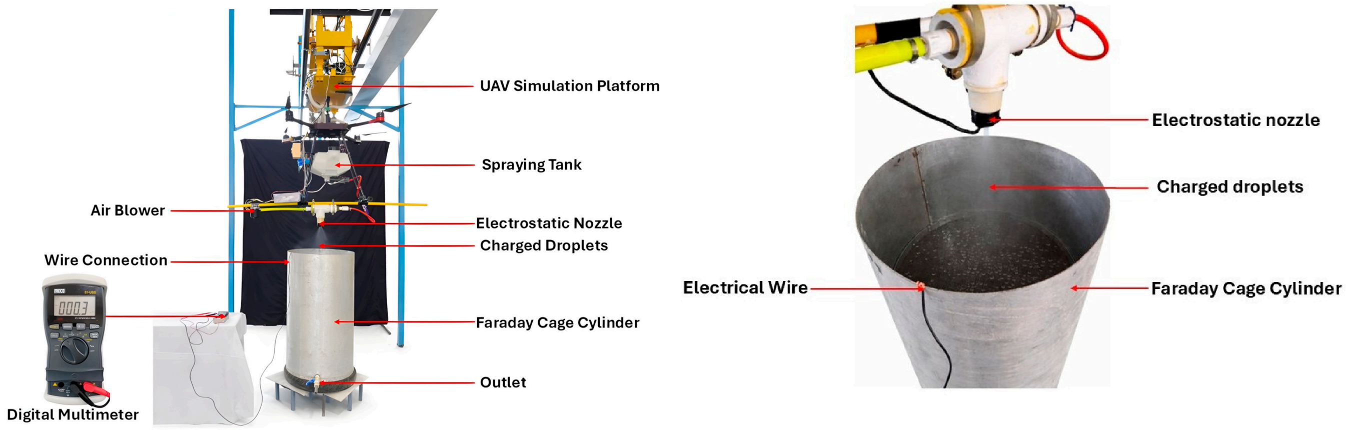

(**a**) (**b**)

Figure 5. Experimental evaluation of the drone-based air-assisted electrostatic spraying system: (**a**) measurement of the CMR using a Faraday cage cylinder; and (**b**) spray nozzle positioning near the cylinder opening during CMR measurement.

2.5.3. Evaluation of the Developed Drone-Based Air-Assisted Electrostatic Spraying System

To evaluate the spray deposition characteristics of charged droplets on a uniform plant target, cotton plants were grown in a vase under laboratory conditions to simulate field conditions. The experiment was conducted by positioning the cotton plants along the travel path of the induction-based air-assisted electrostatic nozzle to investigate the effects of FS, PS, AV, and DR on droplet density (drops/cm^2) (Figure 6a). These operational parameters were selected for optimization, owing to their significant influence on spray efficiency and droplet distribution. Under the charged spraying condition, the effects of FS (2.5, 5.0, and 6.3 km/h), PS (1000, 2000, and 3000 rpm), DR (488, 525, and 563 mL/min), and AV (5.0, 6.0, and 7.5 kV) on droplet density were evaluated. Under the uncharged spraying condition, the same experimental procedure was followed, except that no electrostatic voltage was applied, and only forward speed, propeller speed, and discharge rate were investigated at the same levels (Table 1).

Table 1. Experimental design of the developed air-assisted electrostatic sprayer.

Mode	Independent Parameter	Level	Value	Replications	Dependent Parameter
Charged	Forward speed, km/h	3	2.5, 5, 6.3	3	Density (drops/cm^2)
	Propeller speed, rpm		1000, 2000, 3000		
	Discharge rate, mL/min		488, 525, 563		
	Applied voltage, kV		5, 6, 7.5		
Uncharged	Forward speed, km/h		2.5, 5, 6.3		
	Propeller speed, rpm		1000, 2000, 3000		
	Discharge rate, mL/min		488, 525, 563		

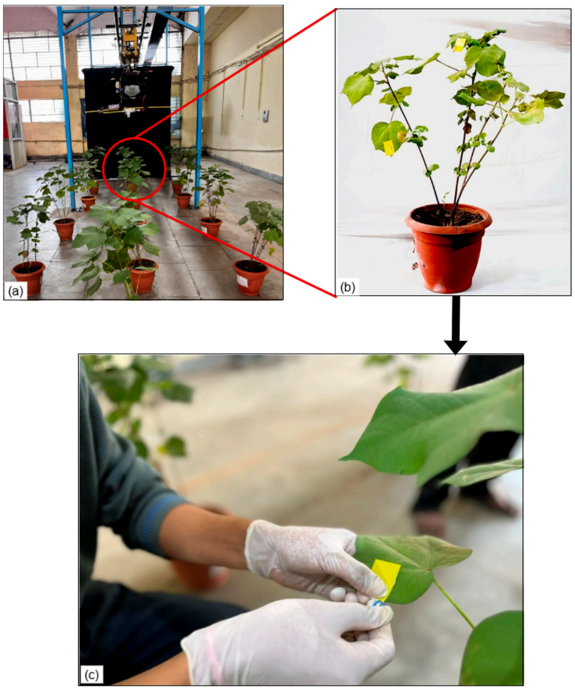

Figure 6. Droplet deposition assessment using an air-assisted electrostatic nozzle. (**a**) Laboratory setup. (**b**) Cotton plant with WSPs at different canopy positions. (**c**) Mounting of WSP on a leaf surface.

For each experimental run, three cotton plants were randomly selected and tagged for sampling. The plants were vertically divided into two canopy zones, namely the bottom zone (0–600 mm above ground level) and the top zone (600–1200 mm above ground level). From each zone, one leaf was randomly selected, and water-sensitive papers (WSPs) (dimensions: 38 × 26 mm; Syngenta Crop Protection, Greensboro, NC, USA) were attached to both the adaxial and abaxial leaf surfaces using paper clips (Figure 6b,c). Each treatment was replicated three times.

Following spraying (Figure 7a), charged spray droplets were deposited onto the WSPs positioned on the adaxial and abaxial surfaces of the cotton canopy (Figure 7b,c).

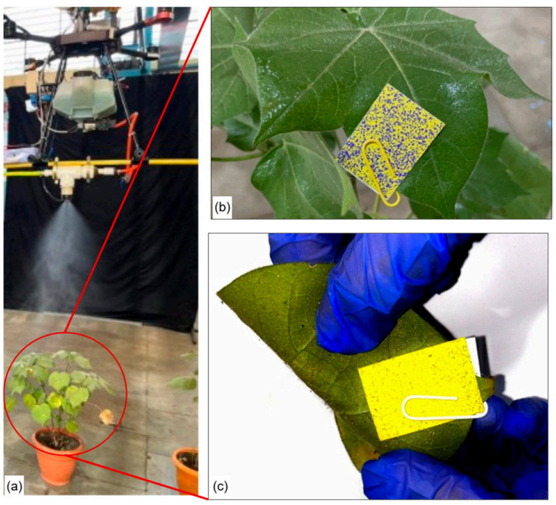

Figure 7. Electrostatic spray deposition on cotton leaves using WSPs. (**a**) Electrostatic spraying under laboratory conditions. (**b**) Droplet deposition on the adaxial (upper) leaf surface. (**c**) Deposition on the abaxial (lower) leaf surface.

The WSPs were allowed to air-dry for 15 min prior to collection. Subsequently, the samples were mounted on labeled sheets, sealed in labeled plastic bags, and preserved in designated envelopes for subsequent droplet density analysis. During the experimental trials, the mean temperature and relative humidity were recorded as 28.5 ± 2 °C and 48 ± 5%, respectively.

2.5.4. Droplet Characterization

The collected WSP samples were scanned at a resolution of 600 dpi using a printer–scanner (model: LaserJet M1136 MFP, Hewlett-Packard, Palo Alto, CA, USA). The scanned images were systematically labeled and organized using Microsoft Photos (version: 2026, Microsoft Corporation, Redmond, Washington, DC, USA). A total of 648 WSP images were generated and annotated. These labeled images were compiled to develop a comprehensive image dataset. Image analysis was performed using the DepositScan (version: DepositScan v1.1, DepositScan, Wooster, OH, USA) plugin in ImageJ (version: ImageJ 1.x series, ImageJ, Bethesda, MD, USA) (Figure 8). Each annotated image was calibrated for pixel dimensions and subsequently converted into 8-bit format [44]. Threshold values were determined using the standard thresholding function available in ImageJ, which accounted for streak patterns generated by wind effects to improve analytical accuracy. The processed images were then converted into binary format to facilitate extraction of droplet characteristics. The analysis primarily focused on droplet density, expressed as the number of droplets per square centimeter (drops/cm^2).

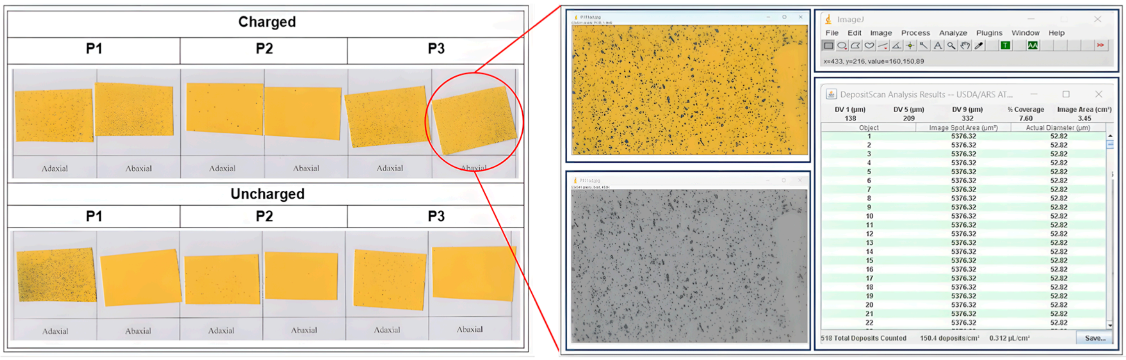

Figure 8. Droplet density analysis of WSPs in ImageJ Software.

2.6. ANN–ACO Modeling

Droplet density of charged spray droplets was affected by FS, PS, DR and AV, as given in Table 1. These independent and dependent parameters were used for mapping droplet density of charged and uncharged sprayed droplets using ANN–ACO modeling. A total of 81 input combinations were generated using a full factorial experimental design for determining the droplet density of charged and uncharged spray droplets. Both independent and dependent variables were replicated three times, and the mean values of the output responses were considered for ANN-based droplet density modeling. A multilayer feed-forward backpropagation ANN, consisting of input, hidden, and output layers [46], was selected for mapping droplet density (Figure 9). The ANN architecture 4-7-13-1 was selected through a trial-and-error optimization process, in which several network configurations with different numbers of hidden layers and neurons were evaluated (Figure 9). The selection was based on achieving the best predictive performance, considering the highest coefficient of determination (R^2) and the lowest prediction errors (RMSE and MAE), while avoiding unnecessary network complexity. The architecture comprises 4 input neurons (discharge rate, forward speed, propeller speed, and applied voltage), two hidden layers with 7 and 13 neurons, and 1 output neuron corresponding to the predicted response.

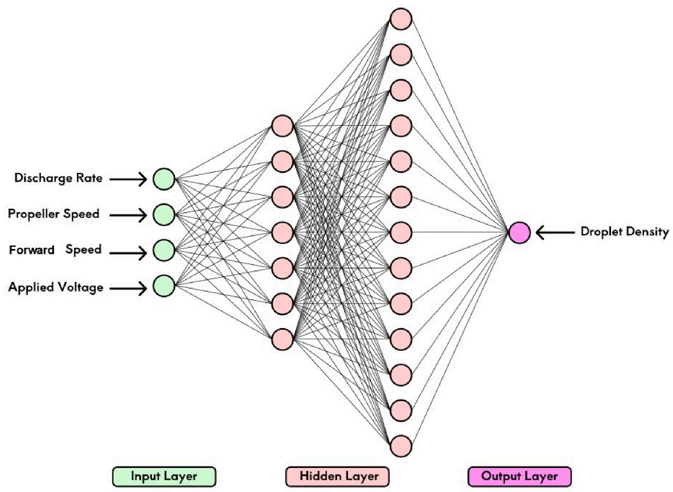

Figure 9. ANN architecture showing input, hidden, and output layers with weighted connections.

The ANN model was developed using MATLAB (version: MATLAB 2019b, MathWorks, Natick, MA, USA) and its Neural Network Toolbox. The developed ANN was trained using an experimental dataset comprising 81 observations, of which 72 datasets (90% of the total dataset) were used for training, while the remaining 9 datasets (10% of the total dataset) were used for testing and validation.

To evaluate and minimize the possibility of overfitting, the dataset of 81 samples was divided into 72 samples for training and 9 independent samples for testing. Prior to training, all input and output variables were normalized to improve training stability and prevent variables with larger numerical ranges from dominating the learning process. In addition, a bagging (bootstrap aggregating) approach was employed, in which multiple neural networks were trained on bootstrap samples generated from the training dataset, and their predictions were averaged. This ensemble technique reduces model variance and improves generalization, making it particularly suitable for relatively small datasets.

The performance of the developed ANN model was evaluated using the coefficient of determination (R^2), root mean square error (RMSE), and mean absolute error (MAE), as described in Equations (2)–(4):

$$R^2 = 1 - \frac{\sum_{i=1}^{N}\left(y_{ai} - y_{pi}\right)^2}{\sum_{i=1}^{N}\left(y_{ai} - \overline{y_a}\right)^2} \quad (2)$$

$$RMSE = \sqrt{\frac{\sum_{i=1}^{N}\left(y_{ai} - y_{pi}\right)^2}{N}} \quad (3)$$

$$MAE = \frac{1}{N}\sum_{i=1}^{N}\left|y_{ai} - y_{pi}\right| \quad (4)$$

where, N represents the total number of datasets, y_{ai} and y_{pi} denote the actual and predicted output values of the i^{th} dataset, respectively, and $\overline{y_a}$ represents the mean of the actual output values.

ACO is a nature-inspired optimization technique based on the foraging behavior of ants; wherein optimal paths are identified through pheromone-mediated communication; this was integrated with the ANN model. In this approach, artificial ants probabilistically construct solutions, with paths having higher pheromone concentrations exhibiting a greater likelihood of selection, thereby indicating superior solutions (Figure 10). The pheromone trails are dynamically updated via evaporation, which diminishes their intensity to prevent premature convergence and deposition, which strengthens high-quality solutions. This controlled balance between exploration and exploitation allows ACO to effectively address complex optimization problems [40].

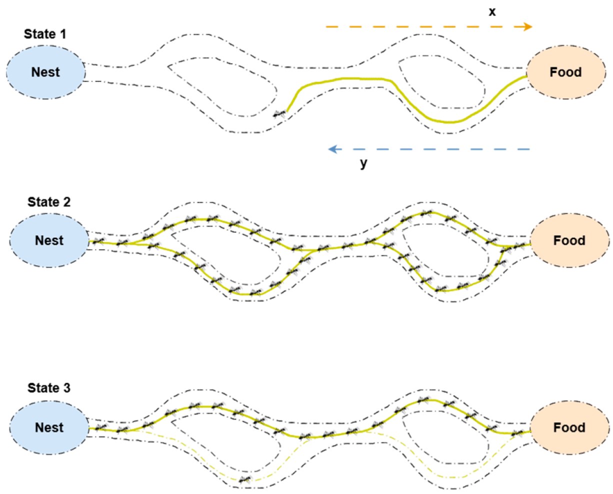

Figure 10. Working principle of ACO.

In MATLAB, prior to training, the dataset was pre-processed through removal of missing values, data conversion, and Min–Max normalization to ensure uniform scaling and improved convergence of the model [51] (Figure 11). The processed dataset was subsequently divided into training (90%) and testing-validation (10%) subsets. The ANN model was trained for 500 epochs to capture complex patterns within the dataset and generate predictive outputs for droplet density corresponding to the independent variables. Model performance was evaluated using RMSE as the fitness criterion, which quantified the deviation between the predicted and observed droplet density values. To further improve prediction accuracy, the weights and biases of the ANN were optimized using the ACO algorithm [52]. In this optimization process, each ant represented a candidate solution corresponding to a specific set of ANN parameters, and pheromone updating was governed by the RMSE-based fitness evaluation. The iterative optimization continued until convergence criteria were satisfied, yielding an optimized ANN model with improved generalization capability. In the testing phase, the optimized ANN model was employed to predict droplet density for various combinations of FS, PS, AV, and DR. The predicted outputs were subsequently analyzed to determine the optimal set of operational parameters that maximize droplet density and improve spray deposition performance. The proposed ANN–ACO framework thus provides a robust and efficient approach for optimizing drone spraying operations. The ACO algorithm was initialized with 30 ants for 50 iterations to where a feasible solution was constructed based on pheromone intensity and heuristic information. The solution was formulated against the objective function with defined constraints. The sole objective was to optimize the operational parameters. The pheromone trails were updated through evaporation and reinforcement that favored an optimal feasible solution of the objective function. The performance evaluation of the ANN–ACO optimization included assessing the basis probabilistic selection of solutions, pheromone intensity and heuristic information, subsequently expressed using Equations (5)–(7):

$$P_{ij} = \frac{(\tau_{ij})^{\alpha}\left(\eta_{ij}\right)^{\beta}}{\sum(\tau_{ij})^{\alpha}\left(\eta_{ij}\right)^{\beta}} \quad (5)$$

$$\tau_{ij}(t+1) = (1-\rho)\tau_{ij}(t) + \Delta\tau_{ij} \quad (6)$$

$$\eta_{ij} = \frac{1}{d_{ij}} \tag{7}$$

where τ_{ij} and η_{ij} denote pheromone intensity and heuristic information, respectively. α and β denote control parameters (commonly $\alpha = 1$, $\beta = 2$). ρ and $\Delta\tau_{ij}$ denote evaporation rate ($0 < \rho \leq 1$) and pheromone deposited, respectively. d_{ij} denotes distance (or cost) between nodes.

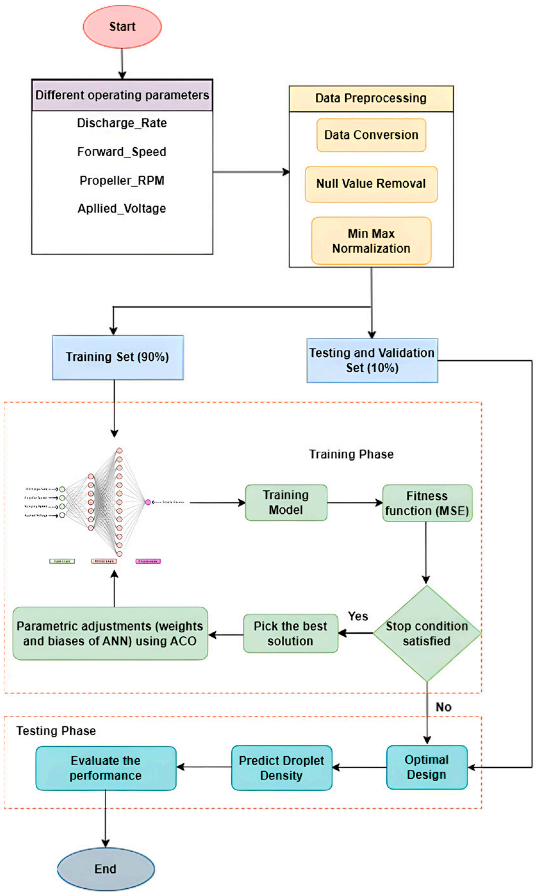

Figure 11. Flowchart of the ACO–ANN hybrid model.

2.7. Data Analysis

Droplet density data were analyzed independently using R software (version: 4.3.0; R Foundation for Statistical Computing, Vienna, Austria). Data normality was initially assessed using quantile-quantile (Q-Q) plots, and where deviations from normality were detected, cube-root transformation was applied to normalize the dataset. Subsequently, a split-split plot multifactor analysis of variance (ANOVA) was performed by considering FS, PS, AV and DR as fixed factors, while droplet density was treated as the response variable.

For factors or interactions containing three or more levels that showed significant effects in the ANOVA, post hoc mean comparisons were conducted using Tukey's honestly significant difference (HSD) test through the HSD.test function available in the agricolae package. In addition, line graphs were generated to visually demonstrate the relative influence of each operational parameter, enabling clear comparison of their effects on the response variable. Statistical significance was determined at both 1% and 5% probability levels.

3. Results and Discussion

3.1. Effect of Different Operating Parameters on Charged Droplet Density

There were four independent operating parameters considered to determine their effect on charged droplet density (drops/cm^2). The independent operating parameters were discharge rate (DR), forward speed (FS), propeller speed (PS) and applied voltage (AV). A total number of 162 experiments were conducted in order to determine the effect of various independent operating parameters on the droplet density.

As shown in the ANOVA (Table 2), the main effects of discharge rate (DR) (F = 50.44, $p < 2 \times 10^{-16}$), forward speed (FS) (F = 13.98, $p = 1.21 \times 10^{-6}$), propeller speed (PS) (F = 4.07, $p = 0.0176$), and applied voltage (AV) (F = 40.37, $p < 2 \times 10^{-16}$) were all statistically significant, indicating that each operating parameter individually influenced the response variable. However, none of the two-way, three-way, or four-way interaction terms were statistically significant (all $p > 0.05$). For example, the interactions DR × FS ($p = 0.9762$), DR × AV ($p = 0.2822$), FS × AV ($p = 0.9129$), and PS × AV ($p = 0.9961$) were all non-significant.

Table 2. ANOVA for the charged droplet density characteristics of drone-based simulation platform at different operating parameters.

Source	Df	Sum Sq	Mean Sq	F Value	Pr(>F)
Discharge rate (DR)	2	366,033	183,016	50.439	$<2 \times 10^{-16}$ ***
Forward speed (FS)	2	101,427	50,714	13.977	1.21×10^{-6} ***
Propeller speed (PS)	2	29,523	14,762	4.068	0.0176 *
Applied voltage (AV)	3	439,444	146,481	40.370	$<2 \times 10^{-16}$ ***
DR × FS	4	1709	427	0.118	0.9762
DR × PS	4	184	46	0.013	0.9997
FS × PS	4	197	49	0.014	0.9996
DR × AV	6	27,077	4513	1.244	0.2822
FS × AV	6	7506	1251	0.345	0.9129
PS × AV	6	2227	371	0.102	0.9961
DR × FS × PS	8	574	72	0.020	1.0000
DR × FS × AV	12	179	15	0.004	1.0000
DR × PS × AV	12	110	9	0.003	1.000
SS × PS × AV	12	79	7	0.002	1.000
DR × FS × PS × AV	24	187	8	0.002	1.000
Residuals	540	1,959,378	3628		

Significance codes: *** $p < 0$, * $p < 0.05$.

The ANOVA results indicate that discharge rate, forward speed, propeller speed, and applied voltage each had significant individual effects on the response, whereas the interaction effects among these operating parameters were not statistically significant ($p > 0.05$), suggesting that the effect of each factor was largely independent of the levels of the other factors within the experimental range investigated.

3.2. Effect of DR on Charged Droplet Density

The results presented in the ANOVA (Table 2) indicate that DR had a significant effect on charged droplet density ($F_{2, 540} = 50.439$, $p < 0.001$). The average charged droplet densities of 64.26 ± 3.26 drops/cm^2, 101.25 ± 4.75 drops/cm^2, and 121.69 ± 5.97 drops/cm^2 were obtained at DR values of 488, 525, and 563 mL/min, respectively (Figure 12a). Figure 12a further illustrates that charged droplet density increased significantly with increasing DR at $p < 0.001$. The lowest charged droplet density was observed at 488 mL/ min, while the highest was obtained at 563 mL/min, with 525 mL/min showing an intermediate response. This trend indicates that increasing the DR enhanced spray deposition per unit area and improved charged droplet density. The different lowercase letters indicate statistically significant differences among treatment means according to Tukey's HSD test ($p < 0.05$).

The significant increase in charged droplet density with increasing DR may be explained by the higher spray flux and greater droplet availability reaching the target surface [8,51]. The denser charged spray cloud formed at higher discharge levels likely improved droplet impaction, retention, and overall deposition efficiency [53–55]. In addition, under electrostatic conditions, increased liquid output may have enhanced charged droplet delivery to the canopy [19].

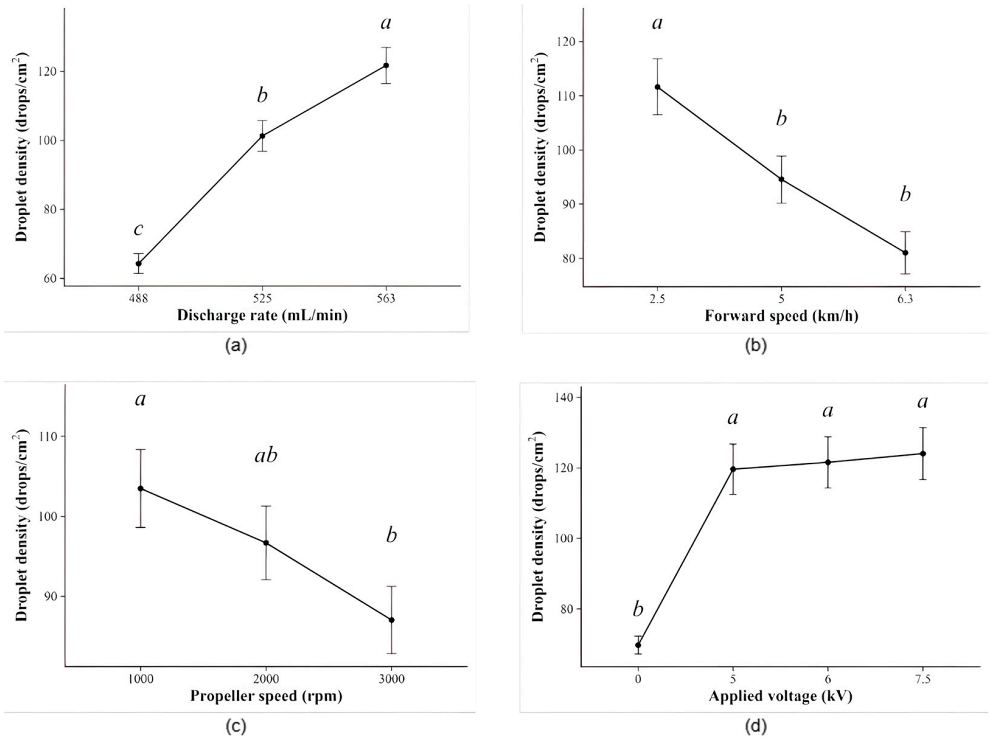

Figure 12. Effect of different operational parameters on droplet density of an air-assisted electrostatic nozzle: (**a**) discharge rate, (**b**) forward speed, (**c**) propeller speed, and (**d**) applied voltage. Distinct letters indicate statistically significant differences among treatment means at $p = 0.05$, as represented by Tukey's honest significant difference test. The error bar indicates standard error.

3.3. Effect of FS on Charged Droplet Density

From the ANOVA results (Table 2), it was observed that FS had a significant effect on charged droplet density ($F_{2,\,540} = 13.977$, $p < 0.001$). As the FS increased from 2.5 to 6.3 km/h, the average charged droplet density decreased from 112.36 ± 5.63 drops/cm^2 to 94.25 ± 4.56 drops/cm^2 and further to 81.14 ± 4.78 drops/cm^2 (Figure 12b). The trend clearly indicates a negative relationship between FS and charged droplet density, as also illustrated in Figure 12b. The reduction in charged droplet density at higher speeds may be attributed to the decreased residence time of droplets within the target zone, resulting in lower deposition on the plant canopy. In contrast, lower FS allows a longer interaction time between charged droplets and the canopy surface, thereby enhancing charged droplet accumulation and increasing overall charged droplet density [9,12,13,56,57].

3.4. Effect of PS on Charged Droplet Density

The ANOVA results (Table 2) indicate that PS had a significant effect on charged droplet density ($F_{2,\,540} = 4.068$, $p < 0.05$). The average charged droplet density decreased from 103.06 ± 5.28 drops/cm^2 at 1000 rpm to 96.57 ± 4.75 drops/cm^2 at 2000 rpm, and further to 87.29 ± 4.97 drops/cm^2 at 3000 rpm (Figure 12c). As illustrated in Figure 12c, charged droplet density exhibited a declining trend with increasing PS. This reduction may be attributed to enhanced airflow velocity and turbulence at higher PS, which can promote droplet drift and reduce deposition on the plant canopy. In contrast, lower PS provides relatively stable airflow conditions with reduced turbulence, facilitating greater droplet retention and improved deposition efficiency on the target surface [57–60].

3.5. Effect of AV on Charged Droplet Density

In the ANOVA results (Table 2) it was found that the AV had a highly significant effect on charged droplet density ($F_{3,\,540} = 40.370$, $p < 0.001$). The average charged droplet density increased from 120.01 $\pm$ 6.75 drops/cm^2 to 124.15 $\pm$ 7.68 drops/cm^2 at an AV of 5 and 7.5 kV, with an intermediate average charged droplet density of 122.10 $\pm$ 7.78 drops/cm^2 at 6 kV (Figure 12d). As illustrated in Figure 12d, beyond 5 kV, the rate of increase was marginal, indicating a plateau effect where further increases in voltage do not substantially enhance charged droplet deposition. The observed improvement in droplet density can be attributed to the increased electrostatic charge imparted to the droplets at higher voltages, which enhances their attraction toward the plant canopy and improves impaction and retention efficiency. The higher voltage likely strengthens the electrostatic forces acting on the droplets, resulting in improved spray deposition and a greater number of droplets deposited per unit area [3,16,28]. The applied voltage range of 5–7.5 kV was selected based on preliminary experiments. At voltages below 5 kV, the measured charge-to-mass ratio (CMR) was less than 1 mC/kg, which is generally inadequate for effective electrostatic agricultural spraying. At voltages above 7.5 kV, the accumulation of charged droplets on the charging electrode initiated back corona discharge, resulting in charge leakage and a reduction in the effective CMR. Therefore, 5–7.5 kV represented the optimum operating range, providing stable charging with an acceptable CMR. The increase in droplet density with applied voltage is attributed to the stronger electrostatic attraction of charged droplets toward the target. However, at higher voltages, the increase became marginal because the CMR increased only slightly (approximately 1.8–2.5 mC/kg) due to reduced charging efficiency caused by charge leakage and the onset of back corona. Consequently, the electrostatic deposition reached a practical limit, resulting in the observed saturation of droplet density at approximately 120 drops/cm^2.

3.6. Optimization of Operational Spray Parameters of a Drone-Based Air-Assisted Electrostatic Spraying System Using a Hybrid ANN–ACO Algorithm

The optimization of spray operational parameters for the drone-based air-assisted electrostatic spraying system was achieved by integrating the best-performing prediction model with the ACO algorithm. The ACO algorithm employed 30 ants and 50 iterations to efficiently explore the operational parameter space associated with droplet density. The convergence curves indicate that the mean droplet density (drops/cm^2) approached the global best values by the 40th and 45th iterations under charged and uncharged conditions, respectively, demonstrating convergence towards the optimal solution (Figures 13 and 14). The ANN–ACO optimization framework was used to analyze droplet density behavior under both charged and uncharged spraying conditions. The optimized operational parameters obtained from the ANN–ACO model was presented in Table 3. The results indicate that forward speeds of 2.58 and 2.80 km/h, discharge rates of 558.45 and 556.75 mL/min, propeller speeds of 1204 and 1065 rpm, and applied voltages of 6.18 and 0.00 kV were optimal for charged and uncharged spraying conditions, respectively. Under these optimized operating conditions, the mean droplet densities achieved were 185.83 $\pm$ 4.25 drops/cm^2 for charged spraying and 108.49 $\pm$ 2.15 drops/cm^2 for uncharged spraying. The integration of predictive ANN models with the ACO optimization algorithm demonstrated an effective approach for improving the droplet density of electrostatic drone systems. Analysis of the convergence curves revealed a progressive enhancement in droplet density, with the mean and global best values showing close agreement, thereby confirming the effectiveness of the

ACO algorithm in identifying optimal operational conditions. The optimized parameter combination maximized charged droplet density, highlighting a systematic framework for fine-tuning drone-based electrostatic spraying systems for agricultural applications. This approach represents an advanced optimization strategy for achieving efficient and precise spray application in modern agricultural practices.

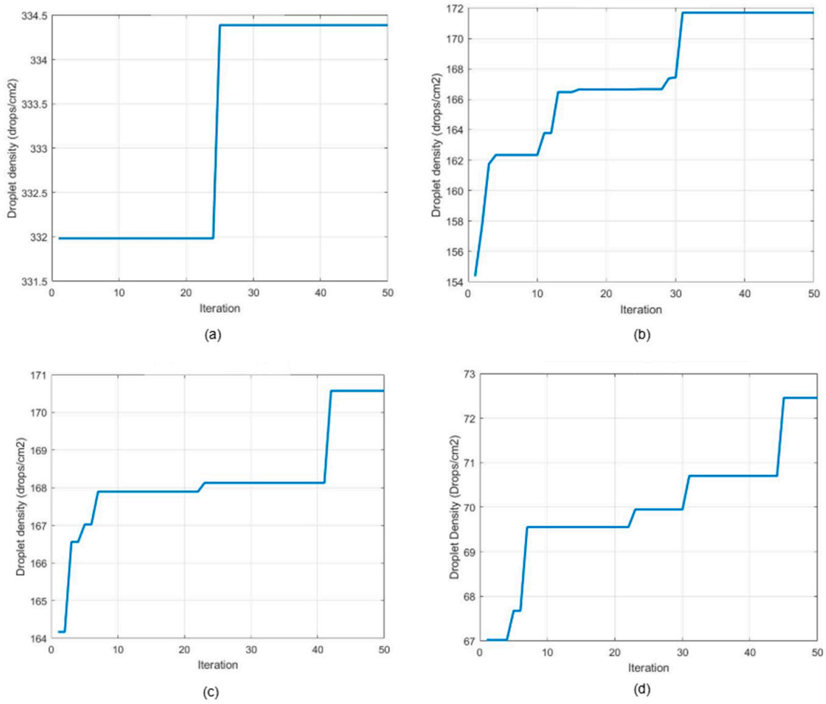

Figure 13. ACO convergence characteristics on charged droplet density on (**a**) top adaxial, (**b**) top abaxial, (**c**) bottom adaxial and (**d**) bottom abaxial.

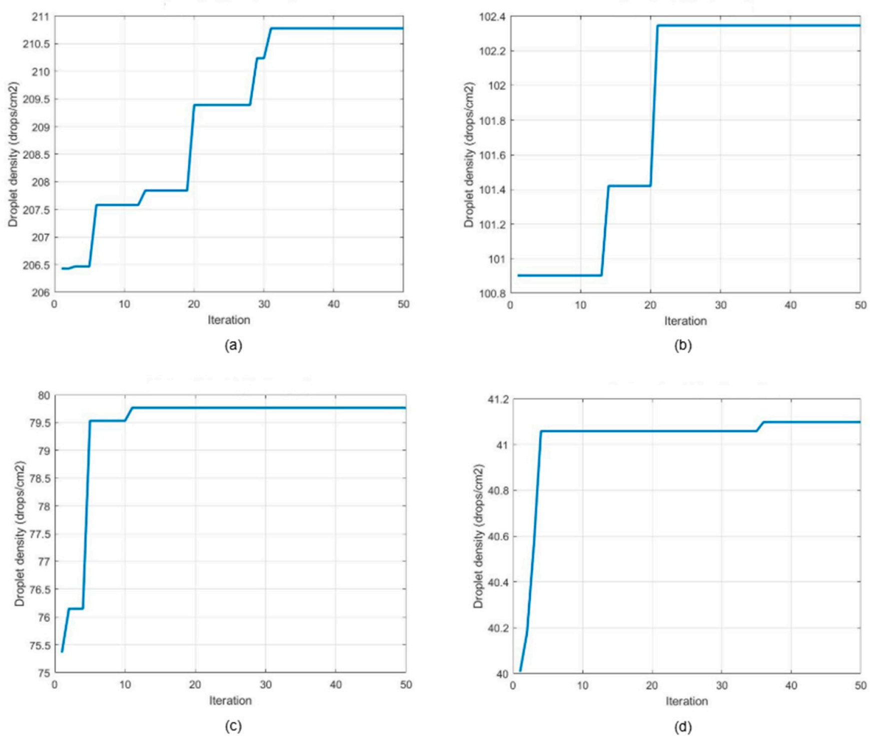

Figure 14. ACO convergence characteristics on uncharged droplet density on (**a**) top adaxial, (**b**) top abaxial, (**c**) bottom adaxial and (**d**) bottom abaxial.

Table 3. Optimized operational parameters obtained using the ANN–ACO model under charged and uncharged spraying conditions.

Mode	FS	PR	DR	AV	Droplet Density		
					Predicted	Observed	Deviation (%)
Charged	2.58	1204	558.45	6.18	185.83	181.58	2.2
Uncharged	2.80	1065	556.75	0.00	108.49	106.34	1.9

The predictive capability of the ANN model was assessed under both charged and uncharged spraying conditions across different canopy zones and leaf surfaces (Table 4). The model exhibited high prediction accuracy, with R^2 values ranging from 0.9740 to 0.9986, indicating strong agreement between the predicted and observed droplet density values. The ANN model showed comparatively better performance under charged spraying conditions, particularly on the abaxial surface of leaves in the top canopy zone (R^2 = 0.9986, RMSE = 1.2167, and MAE = 0.8650). These results emphasize the effectiveness of electrostatic charging in improving droplet deposition characteristics and enhancing the predictive reliability of the model. In contrast, relatively lower performance was observed under uncharged conditions, especially for the abaxial surface in the top canopy (R^2 = 0.9740, RMSE = 3.1125), suggesting greater variability in droplet distribution due to the absence of electrostatic attraction. Across both spraying modes, the bottom canopy consistently exhibited lower RMSE and MAE values compared to the top canopy, indicating more stable and uniform droplet deposition in lower canopy regions. This may be attributed to reduced environmental disturbances such as airflow turbulence and droplet drift [10,59]. Furthermore, the improved prediction accuracy observed on the abaxial surface under charged conditions confirms the enhanced penetration and wrap-around effect of electrostatically charged droplets, which is critical for effective pest and disease control [28]. Overall, these findings demonstrate that the ANN model is a reliable and robust tool for predicting droplet density in drone-based air-assisted electrostatic spraying systems, with electrostatic charging significantly improving both deposition characteristics and model performance.

Table 4. Statistical evaluation of forecasting models based on denormalized data using absolute error metrics.

Model	Mode	Zone	Adaxial			Abaxial		
			RMSE	MAE	R^2	RMSE	MAE	R^2
ANN	Charged	Top	4.5598	3.0123	0.9950	1.2167	0.8650	0.9986
		Bottom	1.5189	0.7707	0.9978	0.6876	0.4680	0.9971
	Uncharged	Top	2.6525	1.9545	0.9953	3.1125	2.4435	0.9740
		Bottom	1.5485	1.1698	0.9899	0.5175	0.3852	0.9955

3.7. Limitations and Future Scope

This study has certain limitations. All experiments were performed under controlled laboratory conditions using a drone-based simulation platform, which may not entirely represent the variability encountered under field conditions, including the influence of wind velocity, relative humidity, and microclimatic fluctuations on droplet dynamics in cotton crops. In addition, the investigation primarily emphasized engineering performance parameters and did not assess biological efficacy aspects such as pest or disease control, nor verify whether the observed charged droplet characteristics satisfy agronomic performance thresholds. The primary objective of the present study was to develop and optimize an ANN–ACO framework for predicting droplet density under controlled laboratory conditions using a drone-based simulation platform. Therefore, the spray height was kept constant to isolate the effects of the selected operating parameters (discharge rate, forward speed, propeller speed, and applied voltage) and to minimize experimental variability. Similarly, external air currents were intentionally excluded to ensure repeatable experimental conditions and to establish the fundamental relationships between the operating parameters and droplet deposition. We agree that varying spray height and incorporating different wind speeds and directions would provide a more comprehensive assessment of the system under practical field conditions.

Future studies should focus on validating the present findings through large-scale field experiments under diverse environmental conditions to evaluate spray performance and model robustness under practical operating scenarios. Incorporation of biological efficacy assessments linking charged droplet deposition characteristics with pest and disease suppression would further strengthen the agronomic significance of drone-based electrostatic spraying systems. Moreover, the adoption of multi-objective optimization techniques to simultaneously enhance spray deposition efficiency and minimize chemical usage could contribute towards the development of sustainable and field-deployable drone-based electrostatic spraying technologies.

4. Conclusions

The present study demonstrated that the performance of the drone-based air-assisted electrostatic spraying system is governed primarily by the operating parameters of discharge rate, applied voltage, forward speed, and propeller speed. Statistical analysis confirmed that discharge rate (F = 50.439, $p < 0.001$) and applied voltage (F = 40.370, $p < 0.001$) were the dominant factors influencing droplet density, followed by forward speed (F = 13.977, $p < 0.001$) and propeller speed (F = 4.068, $p < 0.05$), while the interaction effects among these parameters were not statistically significant. The developed electrostatic charging system produced a stable charge-to-mass ratio (CMR) of 1.8–2.5 mC/kg, which significantly enhanced droplet deposition compared with uncharged spraying. The present study demonstrated that the performance of the drone-based air-assisted electrostatic spraying system is governed primarily by the operating parameters of discharge rate, applied voltage, forward speed, and propeller speed. Statistical analysis confirmed that discharge rate (F = 50.439, $p < 0.001$) and applied voltage (F = 40.370, $p < 0.001$) were the dominant factors influencing droplet density, followed by forward speed (F = 13.977, $p < 0.001$) and propeller speed (F = 4.068, $p < 0.05$), while the interaction effects among these parameters were not statistically significant. The developed electrostatic charging system produced a stable charge-to-mass ratio (CMR) of 1.8–2.5 mC/kg, which significantly enhanced droplet deposition compared with uncharged spraying.

The hybrid ANN–ACO framework successfully modeled the nonlinear relationship between the operating parameters and droplet density, achieving high predictive accuracy (R^2 up to 0.9986) with low prediction errors. Optimization identified 2.58 km/h forward speed, 558.45 mL/min discharge rate, 1204 rpm propeller speed, and 6.18 kV applied voltage as the optimum operating conditions, resulting in a predicted droplet density of 185.83 drops/cm^2, which was approximately 71% higher than that obtained under optimized uncharged spraying (108.49 drops/cm^2). These findings demonstrate that integrating electrostatic charging with data-driven optimization provides a scientifically robust approach for improving spray deposition and offers a practical framework for optimizing UAV-based precision pesticide application.

Author Contributions: Conceptualization, C.Y.; methodology, S.P.K., B.J., R.K.S.; Experimental design and assistance, S.P., A.S., M.K. (Manish Kumar); Data curation, C.Y., M.K. (Manoj Kumar), K.S.; Writing—original draft preparation, C.Y., B.J., S.P.K.; Writing—review and editing, C.Y., R.K.S., Supervision, K.N.A., K.S. All authors have read and agreed to the published version of the manuscript.

Funding: This research received no external funding.

Data Availability Statement: The data presented in this study are available on request from the corresponding author.

Acknowledgments: The authors express their gratitude to the Director of ICAR-CIAE Bhopal and the Head of CEAAA at ICAR-CIAE, Bhopal, for providing research facilities, infrastructure, financial assistance, and insightful guidance throughout this research endeavor. Research was supported by the Indian Council of Agricultural Research, Department of Agricultural Research and Education, Government of India.

Conflicts of Interest: The authors declare no conflicts of interest.

References

1. Calderone, G.; Ferro, M.V.; Catania, P. A systematic literature review on recent unmanned aerial spraying systems applications in orchards. *Smart Agric. Technol.* **2025**, *10*, 100708. [CrossRef]
2. Mamidi, V.R.; Ghanshyam, C.; Manoj Kumar, P.; Kapur, P. Electrostatic hand pressure knapsack spray system with enhanced performance for small scale farms. *J. Electrostat.* **2013**, *71*, 785–790. [CrossRef]
3. Jyoti, B.; Mani, I.; Kumar, A.; Khura, T.K. Studies on chargeability parameters of charged spray droplets for chemical application in agriculture. *Indian J. Agric. Sci.* **2020**, *90*, 1245–1249. [CrossRef]
4. Prakash, S.K.; Kumar, M.; Jat, D.; Jyoti, B.; Subeesh, A.; Agrawal, K.N.; Tiwari, P.; Mehta, C.R.; Singh, P.L.; Singh, K.K. *Applications of Drones in Agriculture: Status and Scope*; Indian council of agricultural Research: New Delhi, India, 2022.
5. Yumnam, C.; Marak, A.B.; Kumar, M.; Khatri, S.; Kumar, S.; Soni, S.; Kabil, K.; Balaji, V.; Sahni, R.K.; Kumar, S.P.; et al. Utilising drones in agriculture: A review on remote sensors, image processing and their application. *Mod. Agric.* **2025**, *3*, e70021. [CrossRef]
6. Talaeizadeh, A.; Sharifi, I.; Alasty, A.; Ghatrehsamani, S. Agricultural spraying drones: A comprehensive review. *Smart Agric. Technol.* **2025**, *12*, 101519. [CrossRef]
7. Sahni, R.K.; Kumar, S.P.; Thorat, D.; Sanodiya, R.; Soni, S.; Yumnam, C.; Chaudhary, V.P. Comparative assessment of the efficacy of drone spraying and gun spraying for nano-urea application in a maize crop. *Drones* **2026**, *10*, 1.
8. Kumar, S.P.; Jat, D.; Sahni, R.K.; Jyoti, B.; Kumar, M.; Subeesh, A.; Parmar, B.S.; Mehta, C.R. Measurement of droplets characteristics of UAV based spraying system using imaging techniques and prediction by GWO-ANN model. *Measurement* **2024**, *234*, 114759. [CrossRef]
9. Ahmad, F.; Qiu, B.; Dong, X.; Ma, J.; Huang, X.; Ahmed, S.; Chandio, F.A.; Han, Y. Effect of operational parameters of UAV sprayer on spray deposition pattern in target and off-target zones during outer field weed control application. *Comput. Electron. Agric.* **2020**, *172*, 105350. [CrossRef]
10. Qi, W.; Chen, P. Analysis of the research progress on the deposition and drift of spray droplets by plant protection UAVs. *Sci. Rep.* **2023**, *13*, 14395. [CrossRef]
11. Godyń, A.; Świechowski, W.; Doruchowski, G.; Hołownicki, R.; Bartosik, A.; Sas, K. Spray deposition, drift and equipment contamination for drone and conventional orchard spraying under European conditions. *Agriculture* **2025**, *15*, 2467. [CrossRef]
12. Manjunatha, K.; Savadi, S.; Anilkumar, C.; Adiga, J.D.; Venkatesh, E.; Vanitha, K.; Sushilendra, S. Effects of flight height, flight speed and spray volume of a UAV based spraying system on droplet deposition in cashew trees. *Results Eng.* **2026**, *29*, 109786. [CrossRef]
13. Psiroukis, V.; Kasimati, A.; Nychas, K.; Dagres, K.; Papadopoulos, G.; Anastasiou, E.; Fountas, S. Effect of spraying drone flight parameters on vineyard canopy coverage and droplet deposition. *Smart Agric. Technol.* **2026**, *13*, 101730. [CrossRef]
14. Koo, D.; Henderson, C.A.; Askew, S.D. Agricultural spray drone deposition, Part 1: Methods for high-throughput spray pattern analysis. *Weed Sci.* **2024**, *72*, 816–823. [CrossRef]
15. Gao, J.; Bo, P.; Lan, Y.; Sun, L.; Liu, H.; Li, X.; Wang, G.; Zhang, H. Study on droplet deposition characteristics and application of small and medium crown garden plants sprayed by UAV sprayer. *Front. Plant Sci.* **2024**, *15*, 1343793. [CrossRef] [PubMed]
16. Law, S.E.; Scherm, H. Electrostatic application of a plant-disease biocontrol agent for prevention of fungal infection through the stigmatic surfaces of blueberry flowers. *J. Electrostat.* **2005**, *63*, 399–408. [CrossRef]
17. Patel, M.K.; Sahoo, H.K.; Ghanshyam, C. High voltage generation for charging of liquid sprays in air-assisted electrostatic nozzle system. *IETE J. Res.* **2016**, *62*, 424–431. [CrossRef]

18. Ma, J.; Liu, K.; Chen, C.; Ahmad, F.; Qiu, B. Influence of plant leaf moisture content on retention of electrostatic-induced droplets. *Sustainability* **2021**, *13*, 11685. [CrossRef]
19. Zhao, S.; Castle, G.S.P.; Adamiak, K. Factors affecting deposition in electrostatic pesticide spraying. *J. Electrostat.* **2008**, *66*, 594–601. [CrossRef]
20. Bueno, M.R.; Sousa Alves, G.; Silva, S.M.; Hachiya, T.S.S.; Guimarães, H.T.S.; Costa, G.A.; Campos, A.T.; Carvalho Filho, A. Air assistance and electrostatic spraying in soybean crops. *Agrochemicals* **2024**, *3*, 107–117. [CrossRef]
21. Khatawkar, D.S.; Dharaneedharan, D.; James, P.S. Knapsack air-assisted electrostatic sprayer for agricultural formulations. *CABI Agric. Biosci.* **2024**, *5*, 80.
22. Patel, M.K.; Khanchi, A.; Chauhan, A.; Kumar, A.; Akkireddi, S.R.K.; Jangra, A.; Kanawade, R.; Manivannan, N.; Mitchell, G.R. Real-time measurement of droplet size and its distribution of an air-induced air-assisted electrostatic nozzle. *J. Electrostat.* **2022**, *115*, 103665. [CrossRef]
23. Ou, M.; Dai, S.; Jing, X.; Jia, W.; Dong, X.; Wang, Y.; Li, Y.; Liu, Y.; Wang, Z. Study on spray deposition effect of a new high-clearance air-assisted electrostatic sprayer. *Agriculture* **2025**, *15*, 1331. [CrossRef]
24. Guo, J.; Dong, X.; Qiu, B. Analysis of the factors affecting the deposition coverage of air-assisted electrostatic spray on tomato leaves. *Agronomy* **2024**, *14*, 1108. [CrossRef]
25. Lin, J.; Cai, J.; Ouyang, J.; Xiao, L.; Qiu, B. The influence of electrostatic spraying with waist-shaped charging devices on the distribution of long-range air-assisted spray in greenhouses. *Agronomy* **2024**, *14*, 2278. [CrossRef]
26. Herkins, M.J.; Zhao, L.; Zhu, H.; Jeon, H. CFD modelling of an electrostatic spraying system to optimise pesticide spray efficiency and reduce drift. *Biosyst. Eng.* **2026**, *263*, 104378. [CrossRef]
27. Gan-Mor, S.; Ronen, B.; Ohaliav, K. The effect of air velocity and proximity on the charging of sprays from conventional hydraulic nozzles. *Biosyst. Eng.* **2014**, *121*, 200–208. [CrossRef]
28. Maski, D.; Durairaj, D. Effects of charging voltage, application speed, target height, and orientation upon charged spray deposition on leaf abaxial and adaxial surfaces. *Crop Prot.* **2010**, *29*, 134–141. [CrossRef]
29. Patel, M.K.; Praveen, B.; Sahoo, H.K.; Patel, B.; Kumar, A.; Singh, M.; Nayak, M.K.; Rajan, P. An advance air-induced air-assisted electrostatic nozzle with enhanced performance. *Comput. Electron. Agric.* **2017**, *135*, 280–288. [CrossRef]
30. Brentjes, A.; Jansen, B.; Pozarlik, A.K. Spray characteristics of an air-assisted electrostatic atomiser. *J. Electrostat.* **2022**, *115*, 103654. [CrossRef]
31. Li, Y.; Li, Q.; Hu, J.; Liu, C.; Zhao, S.; Zhang, W.; Wang, Y. An experimental study on the charging effects and atomization characteristics of a two-stage induction-type electrostatic spraying system for aerial plant protection. *Agronomy* **2025**, *15*, 1641. [CrossRef]
32. Dai, S.; Zhang, J.; Jia, W.; Ou, M.; Zhou, H.; Dong, X.; Wang, Y.; Qiu, B. Experimental study on the droplet size and charge-to-mass ratio of an air-assisted electrostatic nozzle. *Agriculture* **2022**, *12*, 889. [CrossRef]
33. Zhou, H.; Ou, M.; Dong, X.; Zhou, W.; Dai, S.; Jia, W. Spraying performance and deposition characteristics of an improved air-assisted nozzle with induction charging. *Front. Plant Sci.* **2024**, *15*, 1309088. [CrossRef] [PubMed]
34. Zhang, L.; Li, Z.; Chu, H.; Chen, Q.; Li, Y.; Liu, X. Design and evaluation of a novel efficient air-assisted hollow-cone electrostatic nozzle. *Agriculture* **2025**, *15*, 1293. [CrossRef]
35. Wang, S.; Li, X.; Zhou, H.; Lv, X.; Shen, W. Design and experiment of an aerial electrostatic spraying system for unmanned agricultural aircraft systems. *Appl. Eng. Agric.* **2021**, *36*, 955–962.
36. Hu, H.; Kaizu, Y.; Huang, J.; Furuhashi, K.; Zhang, H.; Xiao, X.; Li, M.; Imou, K. Design and performance test of a novel UAV air-assisted electrostatic centrifugal spraying system. *Int. J. Agric. Biol. Eng.* **2022**, *15*, 34–40. [CrossRef]
37. Zhao, D.; Cooper, S.; Chima, P.; Wang, G.; Zhang, L.; Sun, B.; Zhang, Z.; Fritz, B.K. Development and characterization of a contact-charging electrostatic spray UAV system. *Agriculture* **2024**, *14*, 467. [CrossRef]
38. Xue, X.; Zeng, K.; Li, N.; Luo, Q.; Ji, Y.; Li, Z.; Zhang, X.; Li, X. Parameters optimization and performance evaluation model of air-assisted electrostatic sprayer for citrus orchards. *Agriculture* **2023**, *13*, 1498. [CrossRef]
39. Herkins, M.; Zhao, L.; Zhu, H.; Jeon, H.; Castilho-Theodoro, J. Optimization and evaluation of electrostatic spraying systems and their effects on pesticide deposition and coverage inside dense canopy plants. *Agronomy* **2025**, *15*, 1401. [CrossRef]
40. Martin, D.E.; Latheef, M.A.; Duke, S.E. Gap optimization of electrostatic aerial spray nozzles for low-speed aircraft. *J. Electrostat.* **2022**, *117*, 103714. [CrossRef]
41. Zhao, W.; Duan, L.; Ma, B.; Meng, X.; Ren, L.; Ye, D.; Li, J.; Wang, Y. Applications of optimization methods in automotive and agricultural engineering: A review. *Mathematics* **2025**, *13*, 3018. [CrossRef]
42. Dhakad, S.; Shalunkhe, R.C.; Shukla, K.; Seth, N.; Dabhi, K.L.; Balas, D.B. Optimization of operational parameters for agricultural drone spraying in maize crops. *J. Exp. Agric. Int.* **2025**, *47*, 105–120. [CrossRef]
43. Xing, W.; Cui, Y.; Wang, X.; Shen, J. Optimization of operational parameters of plant protection UAV. *Sensors* **2024**, *24*, 5132. [CrossRef] [PubMed]

44. Rogers, H.; Zebin, T.; Cielniak, G.; De La Iglesia, B.; Magri, B. Deep learning for precision agriculture: Post-spraying evaluation and deposition estimation. *arXiv* **2024**, arXiv:2409.16213.
45. Talaviya, T.; Shah, D.; Patel, N.; Yagnik, H.; Shah, M. Implementation of artificial intelligence in agriculture for optimisation of irrigation and application of pesticides and herbicides. *Artif. Intell. Agric.* **2020**, *4*, 58–73. [CrossRef]
46. Kujawa, S.; Niedbała, G. Artificial neural networks in agriculture. *Agriculture* **2021**, *11*, 497. [CrossRef]
47. Nguyen, D.C.H.; Dandy, G.C.; Maier, H.R.; Ascough, J.C. Improved ant colony optimization for optimal crop and irrigation water allocation by incorporating domain knowledge. *J. Water Resour. Plan. Manag.* **2016**, *142*, 04016025. [CrossRef]
48. Nguyen, D.C.H.; Ascough, J.C.; Maier, H.R.; Dandy, G.C.; Andales, A.A. Optimization of irrigation scheduling using ant colony algorithms and an advanced cropping system model. *Environ. Model. Softw.* **2017**, *97*, 32–45. [CrossRef]
49. Ali, M.; Deo, R.C.; Xiang, Y.; Prasad, R.; Li, J.; Farooque, A.; Yaseen, Z.M. Coupled online sequential extreme learning machine model with ant colony optimization algorithm for wheat yield prediction. *Sci. Rep.* **2022**, *12*, 5488. [CrossRef] [PubMed]
50. Xu, Y.; Li, Q.; Xu, X.; Yang, J.; Chen, Y. Research progress of nature-inspired metaheuristic algorithms in mobile robot path planning. *Electronics* **2023**, *12*, 3263. [CrossRef]
51. Fariz, T.K.N.; Basha, S.S. Enhanced crop yield prediction using a hybrid artificial neural network with coati optimization algorithm. *Results Eng.* **2025**, *28*, 107529. [CrossRef]
52. Babes, B.; Boutaghane, A.; Hamouda, N. A novel nature-inspired maximum power point tracking (MPPT) controller based on ACO-ANN algorithm for photovoltaic (PV) system fed arc welding machines. *Neural Comput. Appl.* **2022**, *34*, 299–317.
53. Martin, D.E.; Latheef, M.A. Aerial electrostatic spray deposition and canopy penetration in cotton. *J. Electrostat.* **2017**, *90*, 38–44. [CrossRef]
54. Gu, C.; Sun, J.; Li, S.; Yang, S.; Zou, W.; Zhai, C. Deposition characteristics of air-assisted sprayer based on canopy volume and leaf area of orchard trees. *Plants* **2025**, *14*, 220. [CrossRef] [PubMed]
55. Lv, M.; Xiao, S.; Tang, Y.; He, Y. Influence of UAV flight speed on droplet deposition characteristics with the application of infrared thermal imaging. *Int. J. Agric. Biol. Eng.* **2019**, *12*, 10–17. [CrossRef]
56. Dai, S.; Ou, M.; Du, W.; Yang, X.; Dong, X.; Jiang, L.; Zhao, X.; Wang, G.; Wang, C. Effects of sprayer speed, spray distance, and nozzle arrangement angle on low-flow air-assisted spray deposition. *Front. Plant Sci.* **2023**, *14*, 1184244. [CrossRef] [PubMed]
57. Huang, X.; Li, Y.; Chen, L.; Wang, K. CFD-based flow field characteristics of air-assisted sprayer in citrus orchards. *Agriculture* **2025**, *15*, 1103. [CrossRef]
58. Xu, X.; Chen, S.; Li, Z.; Wu, Z.; Tan, Y.; Huang, S.; Li, J.; Wang, G.; Wang, C. Distribution characteristics of rotor airflow and droplet deposition of plant protection UAVs under varying rotor–nozzle distances. *Agriculture* **2025**, *15*, 1995. [CrossRef]
59. Singh, J.; Din, M.; Mahapatra, J.; Pagare, V.; Agrawal, K.N.; Jyoti, B. Optimization of spray control parameters for improving performance of the tunnel sprayer. *Results Eng.* **2026**, *30*, 109190. [CrossRef]
60. Li, Y.; Wang, Z.; Qi, P.; Feng, X.; Yang, M.; Zhu, Z.; Su, L.; He, X.; Wang, C. Measuring spray droplet size under unmanned aerial spraying system (UASS) downwash airflow using an image-processing-based liquid immersion method. *Pest Manag. Sci.* **2026**, *82*, 4875–4890. [CrossRef] [PubMed]